Combined interfacial shear rheology and microstructure visualization of asphaltenes at air-water and oil-water interfaces

Yu-Jiun Lin

Department of Chemical and Biomolecular Engineering, Rice University, Houston, Texas 77005

Sourav Barman

Department of Mechanical Engineering, Texas Tech University, Lubbock, Texas 79409-1021

Peng He and Zhuqing Zhang

Department of Chemical and Biomolecular Engineering, Rice University, Houston, Texas 77005

Gordon F. Christopher

Department of Mechanical Engineering, Texas Tech University, Lubbock, Texas 79409-1021

Sibani Lisa Biswal[a)]

Department of Chemical and Biomolecular Engineering, Rice University, Houston, Texas 77005

(Received 19 September 2016; final revision received 18 August 2017; published 3 November 2017)

Abstract

Asphaltenes are surface-active polyaromatic molecules in crude oil that are known to deposit in pipelines or stabilize water droplets by flocculating at interfaces resulting highly viscous emulsions, leading to significant flow assurance problems. Commercial dispersants have been developed to disturb asphaltene aggregation to mitigate deposition, but their role on the interfacial properties of asphaltene films is unclear. In this study, we elucidate asphaltene interfacial rheology at air-water and oil-water interfaces at high and low asphaltene surface coverage and in the presence of dispersants. A modified Langmuir trough with double-wall ring rheometer is used to simultaneously visualize the microstructure of asphaltene interface and measure the rheological responses. Two surface coverages, 0.5 and 4 μg cm^{-2}, show widely different rheological responses at air-water interfaces. Strong yielding behavior was observed for higher coverage while a less yielding behavior and wider linear viscoelastic regime were observed for the lower coverage. Additionally, asphaltenes at decane-water interfaces were less shear-thinning than at air-water interfaces. Surface pressure-area compression-expansion curves show that the interface is more compressible in the presence of commercial chemical dispersants. This combined imaging and interfacial rheology platform provide an effective method to correlate asphaltene microstructure to interfacial rheological properties. © *2017 The Society of Rheology*.
https://doi.org/10.1122/1.5009188

I. INTRODUCTION

Asphaltenes are polyaromatic molecules found in the crude oil and bitumen that are typically characterized by their solubility, where they are soluble in aromatic solvents, such as benzene or toluene, but insoluble in *n*-alkanes. During oil production, asphaltenes can precipitate from crude oil and aggregate due to temperature, pressure, and compositional changes that occur when mixing various oil streams during processing, resulting in pipeline plugging, formation damage, and fouling [1–7]. In particular, asphaltene fouling has been more readily observed during processes involving CO_2 injection for enhanced oil recovery (EOR) [8–12]. Additionally, asphaltenes are known to be surface-active and assemble at oil-water and air-water interfaces, often forming an interfacial film. This leads to flow assurance problems, such as difficulty in transporting highly viscous fluids or separating phases in stabilized water-in-oil emulsions [13,14]. Furthermore, tailings/wastewater containing bitumen and crude oil that are discharged into tailing ponds often deposit and form a film on the pond [15,16]. Therefore, understanding of the interfacial properties of the surface-active species in the oil is essential for recovery and remediation of oils.

More recently, chemical dispersants have been added to disrupt asphaltene aggregation. Dispersants are designed to prevent destabilized asphaltene agglomerates from flocculating and aggregating, keeping them suspended in the crude oil so that they can be carried by the flow instead of depositing onto the surface or plugging pore throats. Previous

[a)]Author to whom correspondence should be addressed; electronic mail: biswal@rice.edu

© 2017 by The Society of Rheology, Inc.

studies of low-molecular-weight alkylbenzene-derived amphiphile dispersants, including alkylphenols and benzenesulfonic acids, describe how increasing the polarity of the head group leads to higher adsorption of amphiphiles on the asphaltenes, while increasing the length of the alkyl tail disrupts asphaltene association [17–19]. Rogel proposed a model for determining the interaction between asphaltenes and chemical dispersants assuming that there is a certain number of active sites allowing the head group (polar moiety) of the dispersant to attach onto asphaltene nanoaggregates [20,21]. Goual *et al*. further found that 4-octylphenol and 4-dodecylphenol tend to form H-bonds at the periphery of asphaltenes, preventing asphaltene aggregation [17]. Therefore, it is of interest to understand how these dispersants alter the interfacial rheology of asphaltenes at the oil-water interfaces.

In the last two decades, the interfacial viscoelasticity of asphaltenes have been studied, including air-water [15,22–31] and oil-water interfaces with either air [32–35] or oil induced aggregation [14,36–43] as well as oil-water interfaces with asphaltenes in the dispersed phase [43–45]. These studies have shown that the conditions by which the asphaltene film forms at the interface determine its rheological responses. Asphaltenes at a heptol-water interface are found to be more compressible than those at an air-water interface [32,33,36]. The rigidity of the film is reduced when maltenes or other demulsifiers are mixed with asphaltenes at the interface, which is thought to reduce the attractive interactions between asphaltenes [24,27]. The addition of solvents to these interfaces alters the interparticle aggregate interactions. It has been observed that low-aromaticity solvents (more aliphatic molecules) increased the attractive interactions, thereby decreasing the time required to saturate the interface with asphaltenes [37].

A Langmuir trough with an existing double wall ring rheometer is modified to perform *in situ* visualization of asphaltene aggregation at air-water and oil-water interfaces while under strain. We relate the observed microstructure of asphaltenes at interfaces with their rheological behavior and in the presence of various chemical dispersants. This allows us to simultaneously visualize dynamic aggregation of asphaltenes at interfaces under various strain conditions. The rheological response is correlated with the microstructure to design more effective chemical additives to mitigate asphaltene related flow assurance problems, and to develop improved remediation methods to recovery discharged oils and bitumen in tailing ponds.

II. MATERIALS AND METHODS

A. Chemicals

The asphaltenes used in this research were extracted by *n*-pentane from Canadian bitumen sample. Asphaltenes extracted from other sources may have different chemical functionalities that alter their rheological response. A solution of model oil was made by weighing the asphaltenes of the desired mass and dissolving 0.5 wt. % asphaltenes in toluene using a 40 kHz ultrasonic bath (VWR) at 90 °C for a minimum of 30 min. Asphaltenes are further characterized by zeta potential and dynamic light scattering (DLS) measurements using Delsamax Pro (Beckman Coulter) as listed in Table S1. The chemical dispersants used are alkylphenols: *p*-octylphenol (purity $\geq$ 99%, Sigma Aldrich) and *p*-dodecylphenol (96.5%, Pfaltz&Bauer). Dispersants are premixed with the asphaltene solution, and the concentration is 0.01 wt. %. All other chemicals were purchased from Sigma Aldrich: *n*-pentane (for HPLC, purity $\geq$ 99%) *n*-heptane (for HPLC, $\geq$ 99%), *n*-decane (anhydrous, $\geq$ 99%), toluene (anhydrous, 99.8%) and used as received. Deionized water (18.2 MΩ cm) was used as the subphase.

B. Interfacial rheology

The rheology of asphaltenes at various interfaces were investigated with an AR-G2 stress-controlled rheometer with an interfacial rheology cell described by Vandebril *et al*. (inner radii are 31 mm for the subphase and 30 mm for the upper phase, and outer radii are 39.5 mm for the subphase and 40.5 mm for the upper phase), based on a double-wall ring geometry (TA instruments) [46]. The rheometer has been modified to allow visualization of the interface during experimentation [47]. Asphaltenes at an air-water interface are prepared by dropwise spreading of the mixture of asphaltene solution (20 vol. %) with *n*-heptane (80 vol. %), which precipitates a significant fraction of the asphaltenes from the solution. Evaporation time for *n*-heptane and toluene is at least 20 min [23,27,32]. Decane is chosen as the oil phase since it is a "poor" solvent for the asphaltenes; therefore, asphaltenes will be driven to the oil-water interface. Asphaltenes at oil-water interfaces were prepared two ways: (1) Spreading 4 ml of *n*-decane dropwise onto the asphaltene layer formed at the air-water interface described previously (decane-water interface with the aggregation in the air, DW-a) or (2) spreading 4 ml of *n*-decane dropwise onto the water subphase and then injecting the asphaltene solution at the decane-water interface (decane-water interface with the aggregation in decane, DW-d). Two methods were chosen since asphaltenes are known to trap solvents, which may alter their interfacial activity.

For interfacial shear rheology, a shear deformation at the interface was applied while the interfacial area remained constant. Shear viscosity of the interface was obtained from steady shear experiments. Surface viscosity was measured at a single shear rate, ranging from 0.001 to 1 s^{-1}, for at least 15 min for each shear rate. A new interface was prepared after a set of steady shear rates. The temperature was held constant at 23 °C. The surface viscosity can be modeled as a function of shear rate, as shown below,

$$\eta(\dot{\gamma}) \propto \dot{\gamma}^{k}, \tag{1}$$

where η, $\dot{\gamma}$, and k are surface viscosity, shear rate, and a constant, respectively. When k is less than 0, then the interface shows a shear-thinning behavior. Additionally, when $k < -1$, the interface shows solid and yielding behavior with the assumption that the steady-state shear stress is independent of shear rate [48,49].

Sagis and Fischer previously demonstrated the use of strain amplitude-sweep experiments to study complex fluid-fluid interfaces [50]. Here, small-amplitude-oscillatory-shear (SAOS) experiments were conducted on asphaltenes at interfaces. A new interface was prepared each time. A sinusoidal shear strain was applied to the interface at an angular frequency, $\omega = 1$ rad s^{-1} and strain amplitudes, ranging from 0.01% to 10%; for frequency-sweep experiments, the angular frequency ranged from 0.1 rad s^{-1} to 10 rad s^{-1} with strain amplitude being 0.05%. The storage modulus, G′, and loss modulus G″, which describe the elasticity and viscosity of the interface, are derived from the resulting out-of-phase response [48,51].

C. Langmuir trough experiments

Interface preparation is similar to that of the interfacial rheology. Surface pressure compression-expansion curves of the various interfaces were obtained using a KSV 2000 (KSV Instruments Ltd., Finland). Compression-expansion experiments of the interface were performed at a fixed speed of 1500 mm^2 min^{-1} and the constant temperature of 23 °C was controlled by a circulating water bath (F25 Julabo, Kutztown, PA). The trough is combined with Brewster angle microscopy (BAM) (Accurion, GmbH, Germany) to monitor the asphaltene microstructure.

D. Image analysis

Interface images were captured using a CCD camera (Pixellink PI-E531MU) and analyzed using ImageJ (NIH) [52]. The complex shape of the asphaltene microstructure was quantitatively described by the fractal dimension and the effective aggregate size. Fractal dimension was calculated by the built-in box counting method [53]. Moreover, the effective aggregate size was calculated by fitting the interfacial area of asphaltenes into a defined circle with diameter, as described in Supplementary Material [54].

III. RESULTS AND DISCUSSION

A. Surface pressure-area compression-expansion curves of asphaltenes at air-water interfaces

Asphaltenes at the air-water interface were subject to two cycles of compression-expansion experiments using a Langmuir trough to obtain plots of surface pressure versus area [Fig. 1(a)]. Also, the corresponding BAM images are shown in Fig. 1(b). In the presence of asphaltenes, the surface pressure was initially negligible, and then upon compression, the surface pressure began to rise once asphaltenes came into closer contact [Figs. 1(b1) and 1(b2)] [15]. The trough area at which this rise occurred corresponds to is 600 cm^2 and considering the mass of the asphaltenes added to the interface was 280 μg, surface pressure started to increase at 0.46 μg cm^{-2}. Further compression resulted in increasing surface pressure, indicative of a 2D continuous "skin" of asphaltenes [Fig. 1(b3)]. As the trough area was further decreased, and surface pressures increased above 35 mN m^{-1}, as a result of asphaltenes jamming together

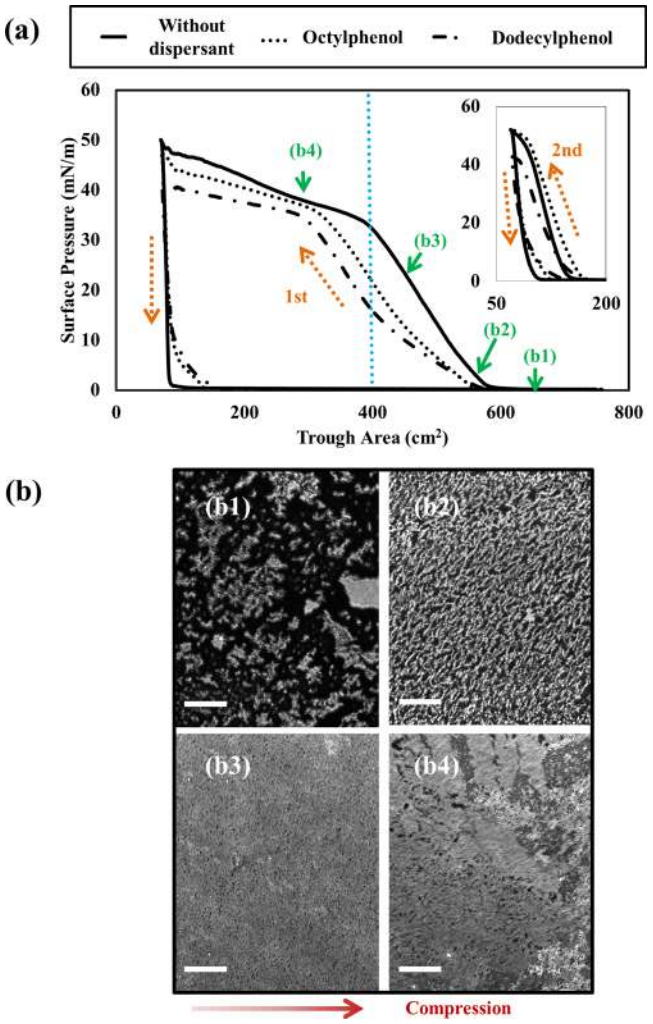

FIG. 1. Behaviors and morphology of asphaltenes at air-water interfaces with a Langmuir trough. (a) Compression-expansion experiments. The inset plot is the second cycle. (b) BAM images for asphaltenes at air-water interface without dispersants under varying surface pressure. (b1) 0.05, (b2) 3, (b3) 25, and (b4) 38 mN m^{-1}. The scale bar is 100 μm.

[15]. Compression of this solid film resulted in instabilities, such as surface wrinkling and multilayer aggregates [Fig. 1(b4)]. Erni *et al.* previously reported temporal alteration of wrinkling and buckling of oil drops in the water solution as a function of oil solubility. They observed a rigid layer at the oil-water interface and concluded that both interfacial compression and shear elasticity were responsible for surface wrinkling [55]. Theo described that wrinkles appeared when particle-laden interfaces were unable to rearrange in-plane, causing them to deform out-of-plane. This also corresponded to the rigidity of the interface [56]. Pauchard *et al.* also observed wrinkles of asphaltenes at interfaces using contracting pendant drop experiments and proposed that this phenomenon was a transition to a glassy interface, comparable to a gelling process [57]. For our asphaltene layer, a max surface pressure was obtained at 48 mN m^{-1} before reaching the limit of the trough compression.

Similar profiles were observed for asphaltenes in the presence of dispersants, as shown in Fig. 1(a), where the rise occurred at 0.46 μg cm^{-2}; however, the surface pressure associated with asphaltenes jamming were lower as a result

of smaller asphaltene aggregates that caused the interface to become more compressible. Furthermore, surface pressure under identical surface coverage decreased following the order of asphaltenes without dispersants, with *p*-octylphenol, and with *p*-dodecylphenol, such that surface pressure was measured as 32.1, 21.6, and 15.3 mN m^{-1}, respectively, when the coverage was 0.7 μg cm^{-2} [the blue dashed line as shown in Fig. 1(a)]. These results indicated that asphaltenes were less capable of reducing the excess free energy of the surface in the presence of the chemical dispersants. As previously described, alkylphenols have been reported to attach onto the periphery of asphaltenes, saturating the H-bond sites (polar moiety) and the alkyl tail further offered more hydrophobicity, suggesting these asphaltenes were less likely to adsorb on the water subphase [17]. Also, there was a large hysteresis upon expansion, where the surface pressure decreases rapidly to zero, due to irreversible aggregation of the asphaltenes at the interface and possible loss of asphaltenes from the interface. The second (and subsequent) cycles showed a much smaller hysteresis. [Fig. 1(a), inset plot].

B. Interfacial rheology of asphaltenes at air-water interface

Rheological behavior of asphaltenes at the air-water interface was examined by steady-shear and SAOS experiments with two surface coverages (0.5 and 4 μg cm^{-2} asphaltenes). The results of the steady-shear viscosity, η, showed characteristic shear-thinning behavior at both coverages [Figs. 2(a) and 2(b)]. The data were fit to Eq. (1) and the power law exponent was obtained. The exponent, k, was determined to be -0.82 (0.5 μg cm^{-2}) and -1.91 (4 μg cm^{-2}), respectively. Additional surface coverage increased the yielding behavior of the interface. Furthermore, asphaltenes mixed with *p*-octylphenol and *p*-dodecylphenol showed lower surface viscosity and a less yielding behavior, with k values being, respectively, -0.69 and -0.61 (0.5 μg cm^{-2}), -1.8 and -1.57 (4 μg cm^{-2}). Dispersants decreased the yielding behavior of the interface likely by disrupting the association of asphaltenes. Goual *et al*. also showed that in the presence of alkylphenols, asphaltene aggregates were observed to be filamentary instead of globular [17].

Furthermore, strain amplitude-sweep results are also shown for these two surface coverages in Figs. 2(c) and 2(d). The rheological response for two coverages varies significantly with strain amplitude. With increasing the surface coverage, both G′ and G″ increased. At the lower coverage, both G′ and G″ remained constant at smaller strain amplitudes and decreased monotonically at larger strain amplitudes. At the higher surface coverage, the interface was more sensitive and brittle to the strain amplitude, and both moduli decreased with increasing strain amplitude. Also, the linear viscoelastic (LVE) regime indicated a more ductile structure at the lower surface coverage (wider LVE) than the higher coverage (narrower LVE). These results will be discussed with corresponding observed microstructures.

In the presence of *p*-octylphenol, both moduli slightly decreased, while with *p*-dodecylphenol both moduli significantly decreased. Also, a similar trend with dispersants was

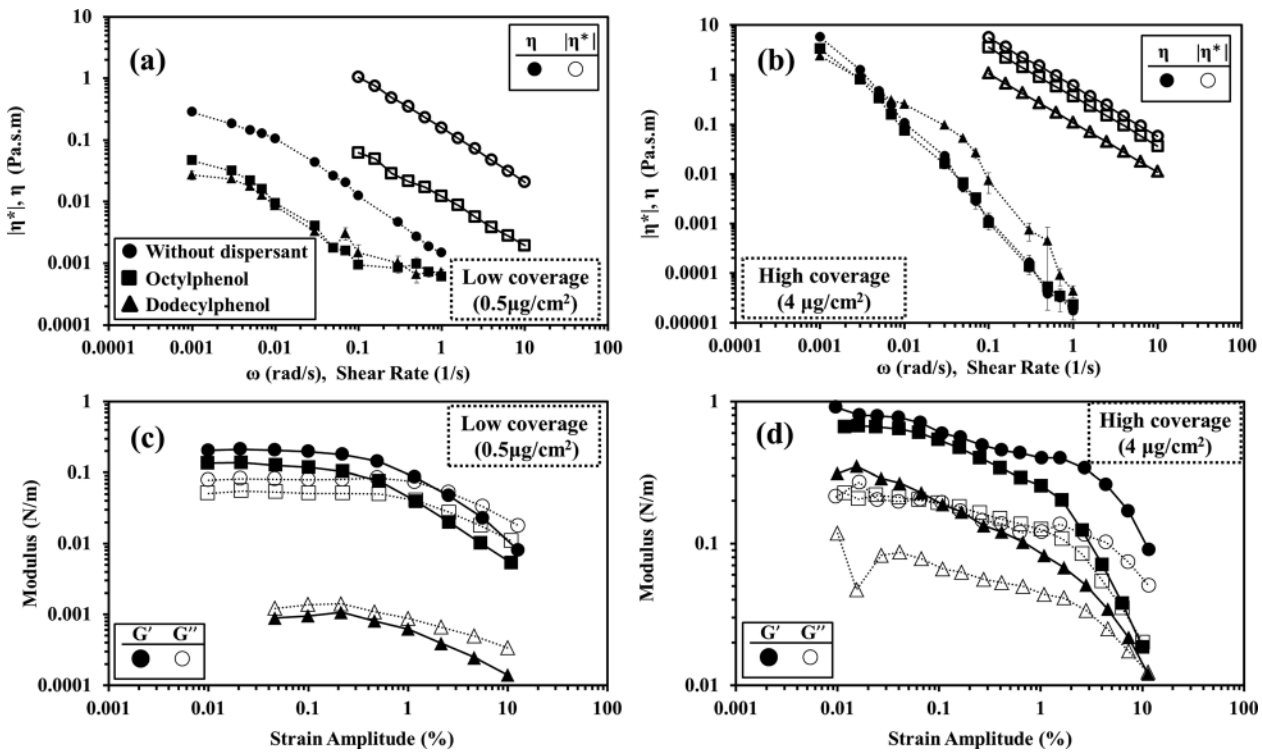

FIG. 2. Rheological behavior of asphaltenes at air-water interfaces. Steady-shear viscosity and dynamic viscosity: (a) 0.5 μg cm^{-2} and (b) 4 μg cm^{-2}. Strain amplitude-sweep experiment: (c) 0.5 μg cm^{-2} and (d) 4 μg cm^{-2}. Black circles correspond to the interface without dispersants, squares are in the presence of *p*-octylphenol, and triangles are in the presence of *p*-dodecylphenol. Averaged G_0' for (c) low coverage = 0.23 ± 0.02 (without dispersants), 0.12 ± 0.04 (*p*-octylphenol) and 0.004 ± 0.007 N m^{-1} (*p*-dodecylphenol). Averaged G_0' for (d) high coverage = 0.85 ± 0.07 (without dispersants), 0.71 ± 0.05 (*p*-octylphenol) and 0.28 ± 0.05 N m^{-1} (*p*-dodecylphenol).

observed in frequency-sweep experiments as shown in Supplementary Material. This response is likely due to phenol molecules disrupting the asphaltene self-association properties, which in turn decreased the elasticity of the asphaltene interface [17,58]. Also, the responses from frequency-sweep experiments showed that the viscoelastic layer (frequency-dependent) was altered to a solid (frequency-independent) film with a higher coverage. Of particular interest is the response with *p*-dodecylphenol at the lower surface coverage that G″ was slightly higher than G′, indicative of a more viscous interface. One possible explanation is that the longer alkyl tail on *p*-dodecylphenol destabilized the association of asphaltenes more readily. However, at the higher coverage, G′ was significantly higher than G″, suggesting a more elastic interface. In this regard, alkyl tails offer greater steric repulsion at the lower surface coverage while they may be more entrained into the multilayer aggregates at the higher surface coverage, shown in Fig. 3(h) and discussed in the following paragraph.

The microscopy images showed the morphological difference between two coverages, where the lower coverage was an asphaltene skin that appeared uniform in grayscale [Fig. 3(a)] while the higher coverage showed jammed multilayer aggregates and surface wrinkling corresponding to a more rigid and solid interface [Fig. 3(b)], which is consistent with the solid response from SAOS results. Tchoukov *et al.* proposed that asphaltenes form a multilayer structure at the oil-water interface based on interferometry measurements [59]. Pauchard *et al.* also described the formation of multilayer asphaltene network is possible due to interactions between the alkyl chains [60]. The asphaltene skin at the low coverage behaved less shear-thinning at a shear rate of $1\ s^{-1}$ and remained unchanged from the microscopy [Fig. 3(e)]. This observation also indicates that the asphaltene skin could possibly reorganize during the experimentation, characteristic of a ductile behavior (wider LVE). However, the skin ruptured for the high surface coverage [Fig. 3(f)]. Multilayer structure remained unaltered, even in the presence of *p*-octylphenol and *p*-dodecylphenol [Figs. 3(c), 3(d), 3(g), and 3(h)] at both shear rates of 0.001 and $1\ s^{-1}$. Erni *et al.* also found that by having a solid yielding layer at air-water interfaces resulted in a shear-thinning response with fractured interface. This fractured layer further gave rise to shear localization, where the interface is only deformed near a spinning disk [61]. The empirical Cox-Merz rule, as shown in Eq. (2), which equates the dynamic viscosity, $|\eta^*(\omega)|$ and steady-shear viscosity, $\eta(\dot{\gamma})$, was also checked [62],

$$|\eta^*(\omega)| = \eta(\dot{\gamma}) \quad with \quad \dot{\gamma} = \omega. \tag{2}$$

For our asphaltene layer, the Cox-Merz rule is not obeyed, with a significant deviation between dynamic and steady-shear viscosity, as shown in Figs. 2(a) and 2(b). Steady-shear viscosity consistently showed lower values than dynamic viscosity. This measured difference further confirmed that the yielding and highly shear-thinning behavior in steady-shear experiments was caused by the fractured interface with the possibility of shear localization, as shown in Fig. 3(f). Moreover, fractured interfaces are not able to reorganize readily, which explains the high sensitivity (narrower LVE) in strain amplitude-sweep experiments when the mechanical strength of the interfacial layer is nonuniform.

C. Interfacial rheology of asphaltenes at oil-water interface

As previously mentioned, a DW-a layer (asphaltenes at the decane-water interface with the aggregation in the air) was prepared by adding decane to an existing asphaltene film at an air-water interface versus a DW-d layer (asphaltenes at the decane-water interface with the aggregation in

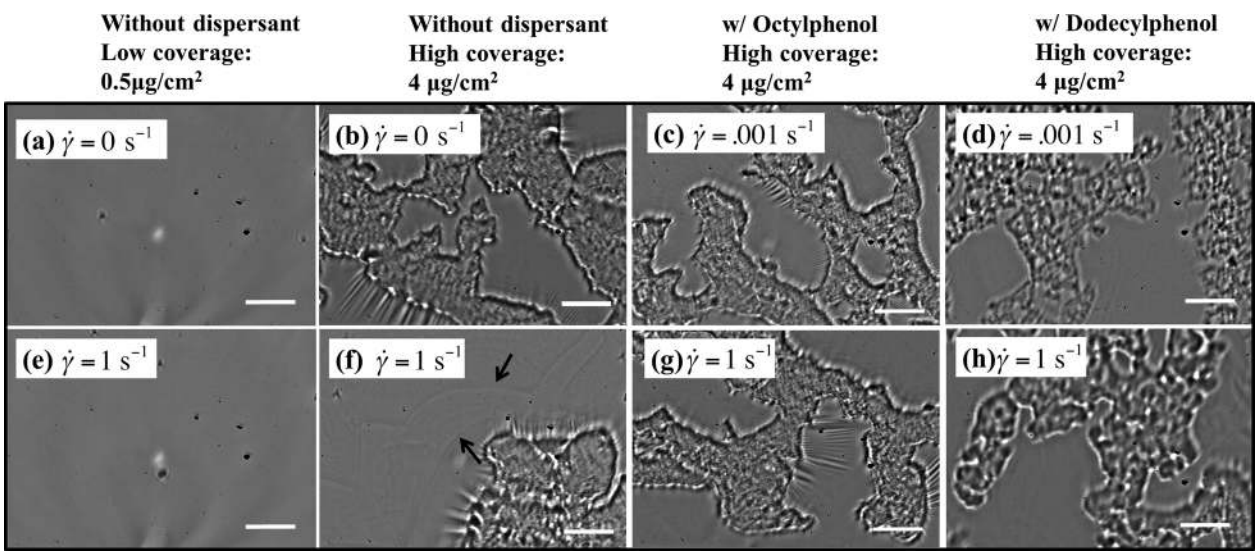

FIG. 3. Optical microscopy images of asphaltene microstructure at air-water interfaces. (a) Interface at rest for surface coverage of $0.5\ \mu g\ cm^{-2}$ shows a uniform asphaltene skin. (b) The interface at rest for surface coverage of $4\ \mu g\ cm^{-2}$ shows a wrinkled asphaltene skin coexisting with multilayer asphaltene aggregates. Asphaltenes under the shear rate of $1\ s^{-1}$ at (e) $0.5\ \mu g\ cm^{-2}$ remain unchanged from microscopy and show a fracture in the skin caused by shear stress at (f) $4\ \mu g\ cm^{-2}$. Asphaltene interfaces for surface coverage of $4\ \mu g\ cm^{-2}$ at shear rates of (c) 0.001 and (g) $1\ s^{-1}$ in the presence of *p*-octylphenol, and (d) 0.001 and (h) $1\ s^{-1}$ in the presence of *p*-dodecylphenol. The total strain is around (a) 0, (b) 0, (c) 0.9, (d) 0.9, (e) 2500, (f) 2500, (g) 2500, and (h) 2500. The scale bar is $50\ \mu m$.

decane) was prepared by first forming a decane-water interface and then injecting the asphaltene solution into the subphase. The microscopy images of asphaltenes at the high coverage are shown in Fig. 4. This high coverage was studied to determine the behavior of the multilayer asphaltene aggregates at oil-water interfaces versus air-water interfaces. The general size and close-packed morphology of multilayer structure for DW-a [Fig. 4(a)] are similar to the one at an air-water interface. However, the surface wrinkling of asphaltenes at air-water interfaces was not observed. Though decane is a poor solvent for asphaltenes, the interface may be able to relax due to some solubilization of the asphaltenes into decane. This is supported by Pauchard *et al*., who showed using pendant drop, surface wrinkles in compressed asphaltene films are relaxed when an equilibrium surface pressure was established between adsorption and desorption of asphaltenes from the interface [57]. Also, Samaniuk *et al*. suggested another possible explanation where the hydrophobic components of asphaltenes resulted in repulsive interactions with hexadecane while attractive interactions in the air [38].

The asphaltene film of DW-d [Fig. 4(b)] appeared morphologically different than that observed at either of an air-water or a DW-a interface. Though the multilayer asphaltene islands of DW-d are similar in size to those observed at an air-water interface, they were less tightly packed compared to asphaltenes at an air-water or a DW-a interface. As shown in the inset, the DW-a aggregate shows a finer grain-like structure with a smooth edge, while DW-d aggregates appear to be more fractal-like with a coarser-grain appearance and rough edges. Since the asphaltene solution was injected directly into a decane-water interface, the solvent aggregated with asphaltenes cannot easily evaporate. Gawrys *et al*. used small-angle-neutron-scattering (SANS) to show that solvent entrainment resulted in a 30%–50% swelling of asphaltene aggregates [63,64]. Swollen asphaltenes entrained with solvents at the interface were unable to form tightly packed layer. Moreover, Duerr-Auster *et al*. studied the aggregation-dependent rheological behaviors of polyglycerol fatty acid ester (PGE), and found that the number of the intermolecular junction points in the structure under varying aggregation process was determined the rheological response. A single layer microstructure which aggregated in the air majorly due to the attractive interactions of the alkyl chains showed a lower viscoelastic modulus, while a bilayer structure formed during the adsorption process showed a higher modulus. However, the amount of adsorbed surfactants depended on the adsorption time is resulting in a difficult comparison between two aggregation processes. In our work, the amount of adsorbed asphaltenes for two methods (aggregation in the air or decane) is similar due to the limited solubility of asphaltenes in decane. Therefore, the determining factor in the rheological response is the intermolecular junction points. In the asphaltene aggregation in decane, solvents are trapped in the structure possibly resulting in less junction points, while the aggregation in the air causes more compact structure and more connections [65]. In the presence of the two phenols, the aggregates were dispersed across the interface as shown in Figs. 4(c) and 4(d). Since the phenols decreased the tendency for asphaltenes to self-associate, the resulting microstructure was more of a fractal structure across the interface. Interfaces of asphaltenes with and without dispersants are illustrated in Fig. 4(e). Asphaltene aggregates consisting of nanoaggregates adsorbed on the subphase forming a densely packed interfacial layer without dispersants, while asphaltene nanoaggregates are more sparsely distributed with dispersants since dispersants are designed to have a polar head attaching on nanoaggregates and a tail offering steric repulsions [17–19].

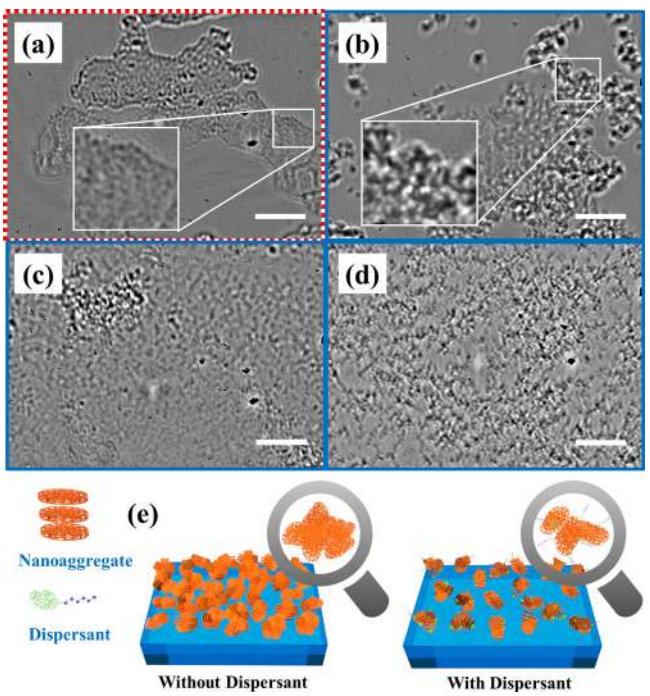

FIG. 4. Asphaltes at decane-water interfaces. (a) DW-a interface. (b) DW-d interface. Insets provide higher resolution microscopy images of the microstructure. (c) DW-d with *p*-octylphenol. (d) DW-d with *p*-dodecylphenol. (e) Illustration of the asphaltenes at interfaces with and without dispersants. All are 4 μg cm^{-2}. The total strain is 0 for all. The scale bar is 50 μm.

The rheological data of asphaltenes without dispersants at air-water and decane-water interfaces for the higher surface coverage are shown in Fig. 5. DW-a ($k = -0.59$) and DW-d ($k = -0.66$) both behaved with a characteristic shear-thinning response, and k is much smaller than that obtained at air-water interfaces [microstructures as shown in Figs. 3(b) and 3(f)]. The Cox-Merz rule is also not obeyed as shown in Fig. 5(a). Complex dynamic viscosity is generally higher than steady-shear viscosity, especially asphaltenes without dispersants at the air-water interface discussed in Sec. III B. However, the dynamic viscosity of DW-a and DW-d are closer to the steady-shear viscosity. The possible explanation is discussed later with microscopy images (Fig. 7) under shear stress. Strain amplitude-sweep results for the various interfaces are shown in Fig. 5(b). The decane-water interface showed much lower moduli than the air-water interface. Reynaert *et al*. also measured aggregated colloidal particles at air-water and decane-water interfaces, and found that the complex viscosity of an air-water interface was much higher than a decane-water interface when varying the surface coverage [66].

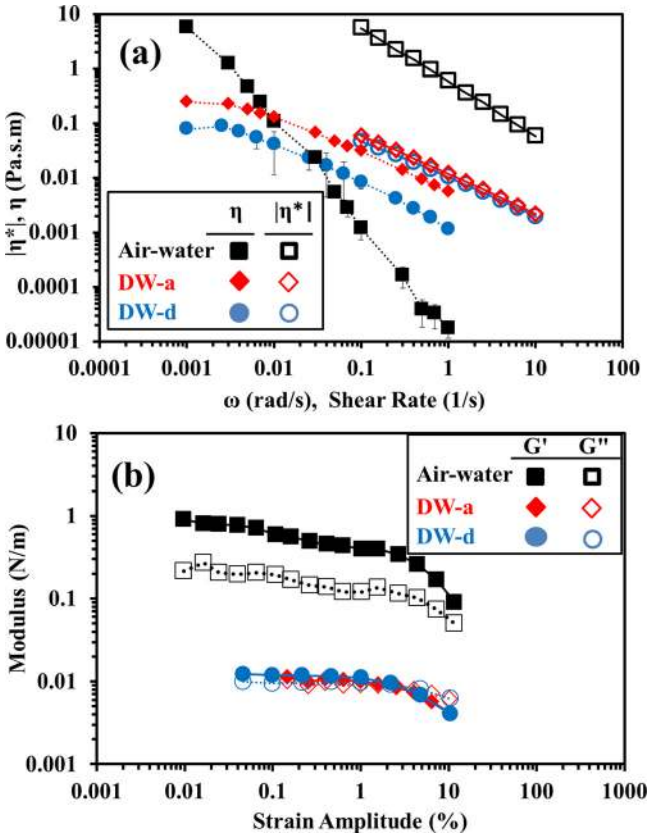

FIG. 5. Rheological properties of asphaltenes at various interfaces without dispersants at a surface coverage of 4 μg cm^{-2}. (a) Steady-shear viscosity and complex dynamic viscosity of different interfaces. (b) SAOS for different interfaces. Squares, diamonds, and circles for asphaltenes at the air-water interface, DW-a, and DW-d, respectively. Averaged G_0' for (b) = 0.85 ± 0.07 (asphaltenes at air-water interface), 0.016 ± 0.004 (DW-a) and 0.015 ± 0.003 N m^{-1} (DW-d).

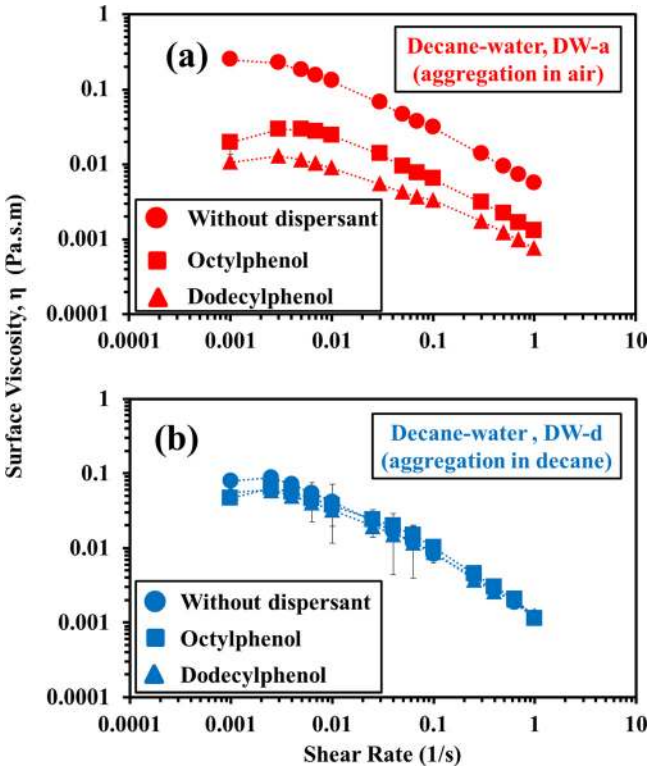

FIG. 6. (a) Steady-shear viscosity of DW-a. (b) Steady-shear viscosity of DW-d. Both are for 4 μg cm^{-2}. Circles, squares, and triangles are for asphaltenes without dispersants, with *p*-octylphenol, and with *p*-dodecylphenol, respectively.

The shear-thinning behavior of decane-water interfaces with dispersants is shown in Fig. 6. With possible desorption of asphaltenes into decane, dispersants were able to disrupt the association of asphaltenes and fluidize the film. This phenomenon also differentiated the influence of dispersants on the steady-shear viscosity, whereby those with a longer alkyl tail caused the asphaltene layer to become more fluidic [Fig. 6(a)]. For DW-d, the behavior of the steady-shear viscosity with and without dispersants was similar. One possible reason is that alkylphenols can partition into the decane phase, thus reducing the interactions between alkylphenols and asphaltenes at the interface [Fig. 6(b)].

As shown in Fig. 7(a), under a shear rate of 1 s^{-1}, the multilayer structure formed on the DW-a separated producing several smaller aggregates at the interface, while no fracture was observed compared to asphaltenes at air-water interfaces. This implies that attractive interactions governing the multilayer structure are much weaker compared to those at air-water interfaces, and the skin around the multilayer structure is able to reorganize during deformation. Interestingly, for DW-d, shown in Fig. 7(b), the multilayer aggregate was dispersed. The governing hypothesis is that solvent entrapment in the DW-d aggregates allows them to be more readily disrupted under a shear stress. Furthermore, the size of shear-dispersed asphaltenes decreased with *p*-octylphenol [Fig. 7(c)], and even smaller with *p*-dodecylphenol [Fig. 7(d)]. In the absence of a fractured interface for both DW-a and DW-d, the possibility of shear localization does not exist, resulting in a less shear-thinning response. These observations could also explain that dynamic viscosity is closer to steady-shear viscosity for decane-water interfaces than the air-water interface, as shown in Fig. 5(a). Shear-induced deformation of the asphaltene layer with dispersants is also shown in Fig. 7(e), illustrating that under shear stress, aggregates are dispersed at the interface.

The rheological properties of the elastic interface have been predicted by the scaling law derived from the concept of the elastic links between aggregates by Shih *et al.* for polymer gels [67]. Reynaert *et al.* used this scaling law, shown in Eq. (3), to characterize 2D particulate suspensions [66],

$$G' \sim \phi^{\nu} \sim \phi^{\frac{d+D_{bb}}{d-D_f}}, \tag{3}$$

where G′ is the elastic modulus, ϕ is the concentration, ν is the power law exponent, d is the dimension of the Euclidean space, D_f is the fractal dimension of the aggregate network, and D_{bb} is the fractal dimension of the backbone of the network. The fractal dimension of the asphaltene aggregates at various interfaces can be calculated under different shear rates, as shown in Fig. 8. The fractal dimension of the multilayer aggregates at the air-water interface remained fairly constant at values between 1.6 and 1.7 for D_f and 1.4 and 1.6 for D_{bb} across various shear rates. For DW-a and DW-d, the

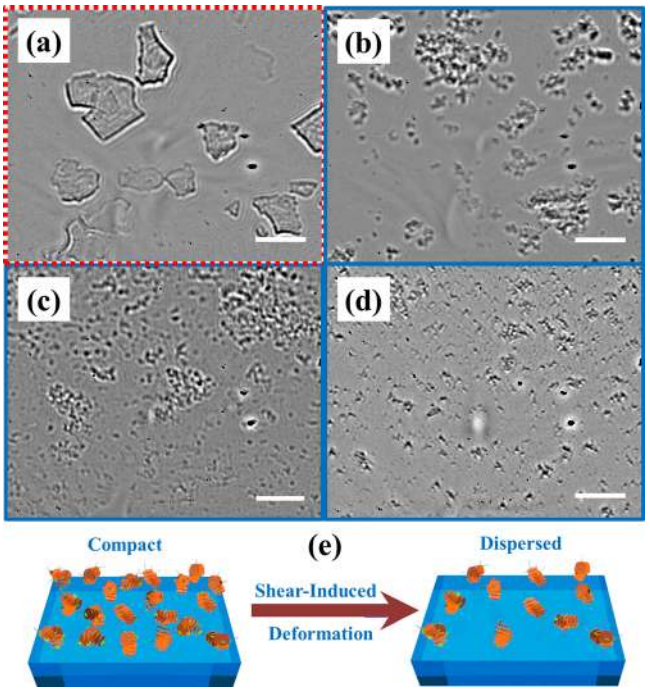

FIG. 7. Asphaltenes under the shear rate of $1\,s^{-1}$ at (a) DW-a without dispersants, (b) DW-d without dispersants, (c) DW-d with *p*-octylphenol, and (d) DW-d with *p*-dodecylphenol. (e) Demonstration of asphaltenes at interfaces before and after shear. All are $4\,\mu g\,cm^{-2}$. The total strain is around 2500 for all. The scale bar is $50\,\mu m$.

fractal dimension decreased to 1.3–1.5 for D_f and 0.9–1.4 for D_{bb}, representing that the interface became more dispersed [Figs. 8(a) and 8(b)]. The power law exponent, v, was within the range of 8.9–9.9 for the air-water interface. Reynaert *et al.* also obtained 8.2 for the network comprised of

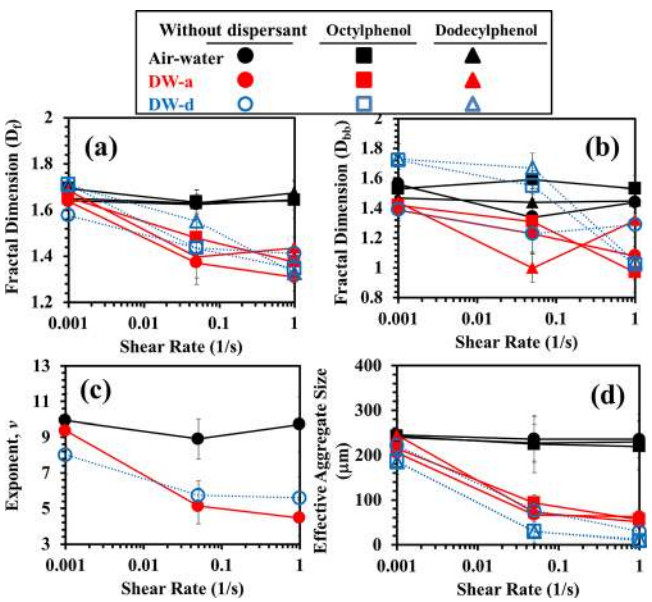

FIG. 8. (a) Fractal dimension of the interfaces with different conditions. (b) Fractal dimension of the backbone of the aggregate network. (c) The power law exponent under various shear rates. (d) The effective aggregate size of the interfaces with different conditions. Circles correspond to the interface without dispersants, squares are in the presence of *p*-octylphenol, and triangles are in the presence of *p*-dodecylphenol.

polystyrene micrometer particles at the air-water interface, which is comparable to our results [66]. The power law exponent decreased with higher shear rates, which matches the decrease of the surface viscosity [Fig. 8(c)]. Moreover, the effective aggregate size was estimated [Fig. 8(d)]. The average size at the air-water interface remained fairly constant but has a large standard deviation while aggregates at the decane-water interface decreased in size with increasing shear stress. Additionally, DW-d aggregates were smaller than DW-a aggregates.

IV. CONCLUSION

Simultaneous analysis of the asphaltene microstructure at interfaces and the corresponding rheological responses was obtained using an interfacial rheometer with the double-wall ring geometry. This method offers a platform to examine the correlation of the asphaltene microstructure to its rheology. Air-water and decane-water interfaces with the aggregation in the air and in decane have been measured. Elastic films, multilayer aggregates, surface wrinkles, and dispersed aggregates were observed. Of particular interest is asphaltenes at the higher surface coverage of $4\,\mu g\,cm^{-2}$, where multilayer aggregates and wrinkles were observed. Fractures were observed during steady-shear experiments, which matches the highly yielding trend with the exponent, $k < -1$. Adding decane as the upper phase altered the asphaltene layer causing surface wrinkles to disappear. Multilayer aggregates were more readily dispersed under the application of a shear stress. The effect of dispersants was also studied and showed that the layer became less elastic. The scaling theory for the correlation between elasticity of the structure and rheological properties was examined. The change of the power law exponent (obtained from the visualization) matched the trend of rheological properties. When the layer was dispersed, the surface viscosity decreased. With the understanding of the correlation of asphaltene microstructure to the rheological responses, the development of a more effective demulsifiers and methods to accelerate the coalescence of the water-in-oil emulsions as well as an improved method for the remediation to recovery crude oil and bitumen discharged in tailing ponds are facilitated.

ACKNOWLEDGMENTS

The authors thank Dr. Mohammad Tavakkoli for the asphaltene extraction and Sang Hun Ji for his technical support.

References

[1] Creek, J. L., "Freedom of action in the state of asphaltenes: Escape from conventional wisdom," Energy Fuels **19**, 1212–1224 (2005).

[2] Vargas, F. M., D. L. Gonzalez, J. L. Creek, J. Wang, J. Buckley, G. J. Hirasaki, and W. G. Chapman, "Development of a general method for modeling asphaltene stability," Energy Fuels **23**, 1147–1154 (2009).

[3] Lin, Y.-J., P. He, M. Tavakkoli, N. T. Mathew, Y. Y. Fatt, J. C. Chai, A. Goharzadeh, F. M. Vargas, and S. L. Biswal, "Examining

asphaltene solubility on deposition in model porous media," Langmuir **32**, 8729–8734 (2016).

[4] Chaisoontornyotin, W., N. Haji-Akbari, H. S. Fogler, and M. P. Hoepfner, "Combined asphaltene aggregation and deposition investigation," Energy Fuels **30**, 1979–1986 (2016).

[5] Chaisoontornyotin, W., A. W. Bingham, and M. P. Hoepfner, "Reversibility of asphaltene precipitation using temperature-induced aggregation," Energy Fuels **31**(4), 3392–3398 (2017).

[6] Zhuang, Y., A. Goharzadeh, Y. J. Lin, Y. F. Yap, J. C. Chai, N. Mathew, F. Vargas, and S. L. Biswal, "Three dimensional measurements of asphaltene deposition in a transparent micro-channel," J. Pet. Sci. Eng. **145**, 77–82 (2016).

[7] Pazuki, G. R., and M. Nikookar, "A modified Flory-Huggins model for prediction of asphaltenes precipitation in crude oil," Fuel **85**, 1083–1086 (2006).

[8] Zeng, Y., A. Muthuswamy, K. Ma, L. Wang, R. Farajzadeh, M. Puerto, S. Vincent-Bonnieu, A. A. Eftekhari, Y. Wang, C. Da, J. C. Joyce, S. L. Biswal, and G. J. Hirasaki, "Insights on foam transport from a texture-implicit local-equilibrium model with an improved parameter estimation algorithm," Ind. Eng. Chem. Res. **55**, 7819–7829 (2016).

[9] Zeng, Y., K. Ma, R. Farajzadeh, M. Puerto, S. L. Biswal, and G. J. Hirasaki, "Effect of surfactant partitioning between gaseous phase and aqueous phase on CO_2 foam transport for enhanced oil recovery," Transp. Porous Media **114**, 777–793 (2016).

[10] Zeng, Y., R. Farajzadeh, A. A. Eftekhari, S. Vincent-Bonnieu, A. Muthuswamy, W. R. Rossen, G. J. Hirasaki, and S. L. Biswal, "Role of gas type on foam transport in porous media," Langmuir **32**, 6239–6245 (2016).

[11] Novosad, Z., and T. G. Costain, *SPE Annual Technical Conference and Exhibition*, New Orleans, LA, 23–26 September (Society of Petroleum Engineers, 1990).

[12] Verdier, S., H. Carrier, S. I. Andersen, and J.-L. Daridon, "Study of pressure and temperature effects on asphaltene stability in presence of CO_2," Energy Fuels **20**, 1584–1590 (2006).

[13] Tavakkoli, M., A. Chen, C.-A. Sung, K. M. Kidder, J. J. Lee, S. M. Alhassan, and F. M. Vargas, "Effect of emulsified water on asphaltene instability in crude oils," Energy Fuels **30**(5), 3676–3686 (2016).

[14] *Encyclopedic Handbook of Emulsion Technology*, edited by J. Sjöblom (Marcel Dekker, New York, 2001).

[15] Hua, Y., and C. W. Angle, "Brewster angle microscopy of Langmuir films of athabasca bitumens, *n* -C5 asphaltenes, and SAGD bitumen during pressure–area hysteresis," Langmuir **29**, 244–263 (2013).

[16] Kotlyar, L. S., J. A. Ripmeester, and B. D. Sparks, "Isolation and characterization of various types of organic matter in oil sands tailings sludge," Fuel **69**, 1522–1526 (1990).

[17] Goual, L., M. Sedghi, X. Wang, and Z. Zhu, "Asphaltene aggregation and impact of alkylphenols," Langmuir **30**, 5394–5403 (2014).

[18] Chang, C.-L., and H. S. Fogler, "Stabilization of asphaltenes in aliphatic solvents using alkylbenzene-derived amphiphiles. 1. Effect of the chemical structure of amphiphiles on asphaltene stabilization," Langmuir **10**, 1749–1757 (1994).

[19] Chang, C.-L., and H. S. Fogler, "Stabilization of asphaltenes in aliphatic solvents using alkylbenzene-derived amphiphiles. 2. Study of the asphaltene-amphiphile interactions and structures using Fourier transform infrared spectroscopy and small-angle x-ray scattering techniques," Langmuir **10**, 1758–1766 (1994).

[20] Rogel, E., "Effect of inhibitors on asphaltene aggregation: A theoretical framework," Energy Fuels **25**, 472–481 (2011).

[21] Hoepfner, M. P., C. Vilas Bôas Fávero, N. Haji-Akbari, and H. S. Fogler, "The fractal aggregation of asphaltenes," Langmuir **29**, 8799–8808 (2013).

[22] Mohammed, R. A., A. I. Bailey, P. F. Luckham, and S. E. Taylor, "Dewatering of crude oil emulsions 2. Interfacial properties of the asphaltic constituents of crude oil," Colloids Surf. Physicochem. Eng. Asp. **80**, 237–242 (1993).

[23] Ese, M.-H., X. Yang, and J. Sjöblom, "Film forming properties of asphaltenes and resins. A comparative Langmuir-Blodgett study of crude oils from north sea, European continent and Venezuela," Colloid Polym. Sci. **276**, 800–809 (1998).

[24] Ese, M.-H., J. Sjöblom, J. Djuve, and R. Pugh, "An atomic force microscopy study of asphaltenes on mica surfaces. Influence of added resins and demulsifiers," Colloid Polym. Sci. **278**, 532–538 (2000).

[25] Cadena-Nava, R. D., A. Cosultchi, and J. Ruiz-Garcia, "Asphaltene behavior at interfaces," Energy Fuels **21**, 2129–2137 (2007).

[26] Zhang, L. Y., S. Lawrence, Z. Xu, and J. H. Masliyah, "Studies of athabasca asphaltene Langmuir films at air–water interface," J. Colloid Interface Sci. **264**, 128–140 (2003).

[27] Álvarez, L., M. E. Díaz, F. J. Montes, and M. A. Galán, "Langmuir technique and Brewster angle microscope studies of the interfacial behavior of bitumen, asphaltenes and maltenes at the air–water interface. I. Effect of different spreading solution volumes," Fuel **89**, 691–702 (2010).

[28] Álvarez, L., M. E. Díaz, F. J. Montes, and M. A. Galán, "Langmuir technique and Brewster angle microscope studies of the interfacial behavior of bitumens, asphaltenes, and maltenes at the air−water interface. 2. Variable spreading solution concentration effect," Energy Fuels **24**, 1771–1780 (2010).

[29] Lobato, M. D., J. M. Pedrosa, D. Möbius, and S. Lago, "Optical characterization of asphaltenes at the air−water interface," Langmuir **25**, 1377–1384 (2009).

[30] Vieira, V. C. C., D. Severino, O. N. Oliveira, F. J. Pavinatto, M. E. D. Zaniquelli, A. P. Ramos, and M. S. Baptista, "Langmuir films of petroleum at the air−water interface," Langmuir **25**, 12585–12590 (2009).

[31] Díaz, M. E., F. J. Montes, and M. A. Galán, "Langmuir films of bitumen and its fractions extracted from oil shales (Puertollano, Spain)," Energy Fuels **21**, 3455–3461 (2007).

[32] Zhang, L. Y., Z. Xu, and J. H. Masliyah, "Langmuir and Langmuir−Blodgett films of mixed asphaltene and a demulsifier," Langmuir **19**, 9730–9741 (2003).

[33] Lawrence, S., L. Y. Zhang, Z. Xu, and J. Masliyah, "Langmuir and Langmuir-Blodgett asphaltene films at heptane-water interface," Can. J. Chem. Eng. **82**, 821–828 (2008).

[34] Zhang, L. Y., R. Lopetinsky, Z. Xu, and J. H. Masliyah, "Asphaltene monolayers at a toluene/water interface," Energy Fuels **19**, 1330–1336 (2005).

[35] Solovyev, A., L. Y. Zhang, Z. Xu, and J. H. Masliyah, "Langmuir films of bitumen at oil/water interfaces," Energy Fuels **20**, 1572–1578 (2006).

[36] Zhang, L. Y., Z. Xu, and J. H. Masliyah, "Characterization of adsorbed athabasca asphaltene films at solvent−water interfaces using a Langmuir interfacial trough," Ind. Eng. Chem. Res. **44**, 1160–1174 (2005).

[37] Spiecker, P. M., and P. K. Kilpatrick, "Interfacial rheology of petroleum asphaltenes at the oil−water interface," Langmuir **20**, 4022–4032 (2004).

[38] Samaniuk, J. R., E. Hermans, T. Verwijlen, V. Pauchard, and J. Vermant, "Soft-glassy rheology of asphaltenes at liquid interfaces," J. Dispers. Sci. Technol. **36**, 1444–1451 (2015).

[39] Harbottle, D., Q. Chen, K. Moorthy, L. Wang, S. Xu, Q. Liu, J. Sjöblom, and Z. Xu, "Problematic stabilizing films in petroleum emulsions: Shear rheological response of viscoelastic asphaltene

films and the effect on drop coalescence," Langmuir **30**, 6730–6738 (2014).

[40] Fan, Y., S. Simon, and J. Sjöblom, "Influence of nonionic surfactants on the surface and interfacial film properties of asphaltenes investigated by Langmuir balance and Brewster angle microscopy," Langmuir **26**, 10497–10505 (2010).

[41] Fan, Y., S. Simon, and J. Sjöblom, "Interfacial shear rheology of asphaltenes at oil–water interface and its relation to emulsion stability: Influence of concentration, solvent aromaticity and nonionic surfactant," Colloids Surf. Physicochem. Eng. Asp. **366**, 120–128 (2010).

[42] Verruto, V. J., R. K. Le, and P. K. Kilpatrick, "Adsorption and molecular rearrangement of amphoteric species at oil−water interfaces," J. Phys. Chem. B **113**, 13788–13799 (2009).

[43] Nenningsland, A. L., S. Simon, and J. Sjöblom, "Influence of interfacial rheological properties on stability of asphaltene-stabilized emulsions," J. Dispers. Sci. Technol. **35**, 231–243 (2014).

[44] Rane, J. P., V. Pauchard, A. Couzis, and S. Banerjee, "Interfacial rheology of asphaltenes at oil–water interfaces and interpretation of the equation of state," Langmuir **29**, 4750–4759 (2013).

[45] Rane, J. P., S. Zarkar, V. Pauchard, O. C. Mullins, D. Christie, A. B. Andrews, A. E. Pomerantz, and S. Banerjee, "Applicability of the Langmuir equation of state for asphaltene adsorption at the oil–water interface: Coal-derived, petroleum, and synthetic asphaltenes," Energy Fuels **29**, 3584–3590 (2015).

[46] Vandebril, S., A. Franck, G. G. Fuller, P. Moldenaers, and J. Vermant, "A double wall-ring geometry for interfacial shear rheometry," Rheol. Acta **49**, 131–144 (2010).

[47] Barman, S., and G. F. Christopher, "Simultaneous interfacial rheology and microstructure measurement of densely aggregated particle laden interfaces using a modified double wall ring interfacial rheometer," Langmuir **30**, 9752–9760 (2014).

[48] Larson, R. G., *The Structure and Rheology of Complex Fluids* (Oxford University, New York, 1999).

[49] Sharma, V., A. Jaishankar, Y.-C. Wang, and G. H. McKinley, "Rheology of globular proteins: Apparent yield stress, high shear rate viscosity and interfacial viscoelasticity of bovine serum albumin solutions," Soft Matter **7**, 5150–5160 (2011).

[50] Sagis, L. M. C., and P. Fischer, "Nonlinear rheology of complex fluid–fluid interfaces," Curr. Opin. Colloid Interface Sci. **19**, 520–529 (2014).

[51] *Rheology: Principles, Measurements, and Applications*, edited by C. W. Macosko (VCH, New York, 1994).

[52] Schneider, C. A., W. S. Rasband, and K. W. Eliceiri, "NIH image to imageJ: 25 Years of image analysis," Nat. Methods **9**, 671–675 (2012).

[53] Fernández, E., J. A. Bolea, G. Ortega, and E. Louis, "Are neurons multifractals?," J. Neurosci. Methods **89**, 151–157 (1999).

[54] See supplementary material at http://dx.doi.org/10.1122/1.5009188 for the analysis of experimental images, frequency-dependent rheological results, and results of the characterization of asphaltenes by Dynamic Light Scattering (DLS) and zeta potential.

[55] Erni, P., H. A. Jerri, K. Wong, and A. Parker, "Interfacial viscoelasticity controls buckling, wrinkling and arrest in emulsion drops undergoing mass transfer," Soft Matter **8**, 6958–6967 (2012).

[56] Kassuga, T. D., and J. P. Rothstein, "Buckling of particle-laden interfaces," J. Coll. Interface Sci. **448**, 287–296 (2015).

[57] Pauchard, V., J. P. Rane, and S. Banerjee, "Asphaltene-Laden interfaces form soft glassy layers in contraction experiments: A mechanism for coalescence blocking," Langmuir **30**, 12795–12803 (2014).

[58] Theodoratou, A., U. Jonas, B. Loppinet, T. Geue, R. Stangenberg, R. Keller, D. Li, R. Berger, J. Vermant, and D. Vlassopoulos, "Semifluorinated alkanes at the air–water interface: Tailoring structure and rheology at the molecular scale," Langmuir **32**, 3139–3151 (2016).

[59] Tchoukov, P., F. Yang, Z. Xu, T. Dabros, J. Czarnecki, and J. Sjöblom, "Role of asphaltenes in stabilizing thin liquid emulsion films," Langmuir **30**, 3024–3033 (2014).

[60] Pauchard, V., J. P. Rane, S. Zarkar, A. Couzis, and S. Banerjee, "Long-term adsorption kinetics of asphaltenes at the oil–water interface: A random sequential adsorption perspective," Langmuir **30**, 8381–8390 (2014).

[61] Erni, P., P. Fischer, P. Heyer, E. J. Windhab, V. Kusnezov, and J. Läuger, "Rheology of gas/liquid and liquid/liquid interfaces with aqueous and biopolymer subphases," in *Mesophases Polymer Particle* (Springer, Berlin, Heidelberg, 2004).

[62] Cox, W. P., and E. H. Merz, "Rheology of polymer melts—A correlation of dynamic and steady flow measurements," in *International Symposium on Plast. Test. Stand.*, Committee D-20 ed. (ASTM International, West Conshohocken, PA, 1959).

[63] Spiecker, P. M., K. L. Gawrys, and P. K. Kilpatrick, "Aggregation and solubility behavior of asphaltenes and their subfractions," J. Colloid Interface Sci. **267**, 178–193 (2003).

[64] Gawrys, K. L., G. A. Blankenship, and P. K. Kilpatrick, "Solvent entrainment in and flocculation of asphaltenic aggregates probed by small-angle neutron scattering," Langmuir **22**, 4487–4497 (2006).

[65] Duerr-Auster, N., R. Gunde, and E. J. Windhab, "Structure and mechanical properties of a polyglycerol ester at the air-water surface," Langmuir **24**, 12282–12289 (2008).

[66] Reynaert, S., P. Moldenaers, and J. Vermant, "Interfacial rheology of stable and weakly aggregated two-dimensional suspensions," Phys. Chem. Chem. Phys. **9**, 6463–6475 (2007).

[67] Shih, W.-H., W. Y. Shih, S.-I. Kim, J. Liu, and I. A. Aksay, "Scaling behavior of the elastic properties of colloidal gels," Phys. Rev. A **42**, 4772–4779 (1990).